communications materials

REVIEW ARTICLE

https://doi.org/10.1038/s43246-022-00327-2 OPEN

Challenges and strategies toward long-term stability of lead-free tin-based perovskite solar cells

Ece Aktas[1], Nagalingam Rajamanickam[2], Jorge Pascual[3], Shuaifeng Hu[3], Mahmoud H. Aldamasy[4], Diego Di Girolamo[1], Wenhui Li[2], Giuseppe Nasti[1], Eugenia Martínez-Ferrero[2], Atsushi Wakamiya[3]✉, Emilio Palomares[2,5]✉ & Antonio Abate[1,4]✉

Due to their outstanding optoelectronic properties, lead-based halide perovskite materials have been applied as efficient photoactive materials in solution-processed solar cells. Current record efficiencies offer the promise to surpass those of silicon solar cells. However, uncertainty about the potential toxicity of lead-based halide perovskite materials and their facile dissolution in water requires a search for new alternative perovskite-like materials. Thanks to the foresight of scientists and their experience in lead-based halide perovskite preparation, remarkable results have been obtained in a short period of time using lead-free perovskite compositions. However, the lower solar-to-energy conversion efficiency and long-term stability issues are serious drawbacks that hinder the potential progression of these materials. Here, we review and analyse strategies in the literature and the most promising solutions to identify the factors that limit the power conversion efficiency and long-term stability of lead-free tin-based perovskite solar cells. In the light of the current state-of-the-art, we offer perspectives for further developing these promising materials.

The current interlaces of geopolitical and environmental crises demand sustainable and efficient energy generation solutions, where new photovoltaic technologies must play a critical role. Hybrid metal-organic halide perovskite solar cells (PSCs) have shown over the years exceptional performances, with the actual efficiency record almost closing the gap with Si-based classical photovoltaic devices[1]. Alas, the environmental toxicity of lead-based compounds and the performance and stability of lead halide PSCs (Pb-HPSCs) still represent massive limitations toward commercialising this technology. Lead is a well-known toxic heavy metal, historically connected to numerous diseases in kids and adults, thus, the exposure to Pb-HPSCs would pose safety concerns if used on a large scale[2].

In the race to substitute lead in PSCs, tin is the first and more promising candidate, due to its low toxicity under different test conditions in comparison to lead[3]. From a physical and theoretical point of view, tin-based halide perovskites (Sn-HPs) have the potential to surpass their lead-based counterparts thanks to their lower bandgap, which is closer to the optimal values determined by the Shockley-Queisser limit[4], high carrier mobility, and low exciton binding energy[5]. On the other hand, the main limitations of Sn-HPs come from the low energy barrier for the oxidation of Sn(II) to Sn(IV), which promotes the formation of an excess of Sn(II) vacancies and the undesired p-doping of the perovskite semiconductor[6, 7]. In fact, Sn-HP materials are still in their infancy. However, the vast amount of knowledge generated during the

[1] Department of Chemical, Materials and Production Engineering, University of Naples Federico II, Piazzale Tecchio 80, 80125 Fuorigrotta, Italy. [2] Institute of Chemical Research of Catalonia (ICIQ-BIST), Av. Països Catalans 16, Tarragona E-43007, Spain. [3] Institute for Chemical Research, Kyoto University, Gokasho, Uji, Kyoto 611-0011, Japan. [4] Helmholtz-Zentrum Berlin für Materialien und Energie GmbH, Hahn-Meitner-Platz 1, 14109 Berlin, Germany. [5] ICREA, E-08010 Barcelona, Spain. ✉email: wakamiya@scl.kyoto-u.ac.jp; epalomares@iciq.es; antonio.abate@helmholtz-berlin.de

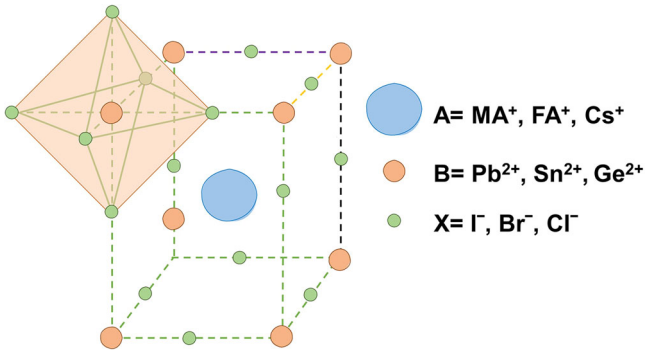

Fig. 1 Scheme of the crystalline structure of 3D perovskite. A depicts monovalent organic or inorganic cations, B represents divalent cations, and X represents halide anions. (Fig. 1 reprinted with permission[135]).

last 15 years in the research of lead halide perovskites, has pushed the research on tin-based halide perovskite solar cells (Sn-HPSCs). They have shown a rapid progression in the achievement of power conversion efficiency (PCE), with the actual record set at 14.6%[8].

A thorough picture of the mechanisms taking place in Sn-HPSCs has not been depicted yet, and its comprehension will be at the base of future improvements for lead-free perovskite devices. In this review, we have collected, analysed, and connected the published reports regarding the factors limiting the PCE and the long-term stability of Sn-HPSCs. After an introductory discussion about the composition engineering of Sn-HPs and the device structures, we have reviewed different approaches adopted to mitigate tin oxidation and promote homogenous film formation. The external agents that can induce degradation of the material, such as humidity, oxygen high temperature, and ultraviolet (UV) light exposure are examined, since their impact on the device performance is detrimental. On the other hand, the intrinsic factors that come into play during the evaluation of the performance of the Sn-HPSCs, such as ion migration leading to significant hysteresis and increased charge recombination, are analysed to provide further information together with the encapsulation procedures to protect the devices. Finally, the Outlook describes the perspectives about the future of Sn-HPSCs and the Conclusions.

Compositional engineering of the lead-free tin-based perovskite

The perovskite constitutes the photoactive part of the solar cells. Its general formula is ABX_3. This general formula of the perovskite structure can be made of different chemical combinations, through the so-called compositional engineering. Thus, A can be an organic cation, generally, methylammonium ($CH_3NH_3^+$, MA^+) or formamidinium ($HC(NH_2)_2^+$, FA^+) or an alkali metal cations such as caesium (Cs^+). B is a divalent metal cation (Pb^{2+}, Sn^{2+}, or Ge^{2+}) whereas X represents the halide anion (I^-, Br^- or Cl^-) (see Fig. 1)[9]. Recently, large organic molecules such as phenethylammonium iodide (PEAI)[10], *n*-propylammonium iodide (PAI)[11] or 4-fluoro-phenethylammonium bromide (FPEABr)[12] have been added into the perovskite precursors to improve the stability of Sn-HPSCs; these larger organic cations block moisture penetration owing to their hydrophobic nature[13]. Furthermore, these large organic cations separate the three-dimensional (3D) perovskites from one another generating low-dimensional perovskite structures like a two-dimensional (2D) or quasi-2D layers. Finally, the perovskites can be found as dots as well, which are described as 0 dimensional (0D), although their applications in Sn-HPs are not the objective of this review.

Sn-HPs are sensitive to ambient conditions that directly affect the efficiency of the devices and their long-term stability. Compositional engineering is one of the most effective approaches to tailor the optoelectronic properties of the Sn-HPs and impact the device stability by reducing the formation of volatile products or irreversible disproportionation when devices are exposed to thermal and light-induced degradation conditions[14, 15]. Hence, in this section, we have summarised the critical contributions reported in regard to the application of different cations to improve the tolerance of the Sn-HPs layer. This review will be focused on the Sn-HPs prepared as 2D or 3D films.

Single cation perovskite. In the 3D Sn-HP structure, the central position, occupied by an organic or alkali metal A site cation (MA^+, FA^+, and Cs^+), heavily influences the resulting electronic properties and the intrinsic stability of the photovoltaic devices prepared with it[16]. Both MA^+ and FA^+ are the most investigated organic cations in position A in lead-free Sn-HPSCs. The comparison between $FASnI_3$ and $MASnI_3$ perovskites indicated that the former, with a larger bandgap[17], showed higher thermal stability due to the larger size of the A-site cation[18]. On the other hand, a systematic comparison of the intrinsic thermal and photochemical stability of a series of Sn-HP layers with three different A-site cations and two halide anions (A = Cs, MA, FA; X = Br, I) was reported by Akbulatov and co-workers in 2019[19]. In their study, the $CsSnI_3$ perovskite composition showed remarkable thermal stability at higher temperature of ~90 °C compared with previously reported hybrid perovskites (FA, MA) and exhibited excellent stability after 1000 h. However, this composition still contained impurities of Cs_2SnI_6 caused by the disproportionation of Sn(II) to Sn^0 and Sn(IV), as indicated by the X-ray diffraction (XRD) patterns (Fig. 2). Therefore, and despite inorganic cation-based $CsSnX_3$ perovskite compositions gave rise to fewer decomposition products due to the absence of fragile and volatile organic cations[20], the operational lifetime of the device was still limited[21].

Double cation perovskite. The introduction of a second A-site cation can affect the electronic structure and the stability of Sn-HPs as has been proven in theoretical and experimental results[17, 22]. In 2017, the photovoltaic performance of double organic cation-based Sn-HPSCs was investigated by Zhao et al.[23]. In their work, the maximum PCE reached 8.12% for the device based on $FA_{0.75}MA_{0.25}SnI_3$, exhibiting high reproducibility. The champion device maintained ≈80% of its original PCE after being stored in N_2 for 400 h (Table 1). Thereafter, Tsai et al. applied an alcohol-based bifunctional ammonium cation, 2-hydroxyethylammonium ($HO(CH_2)_2NH^{3+}$; HEA^+), to modify the energy level of $FASnI_3$ by incorporating HEA^+ in different percentages to the perovskite precursor for boosting the device performance and the stability of lead-free Sn-HPs[24]. It was found that the increment of the HEA^+ cation in the lattice structure of $HEA_xFA_{1-x}SnI_3$ altered the crystal symmetry from orthorhombic ($x = 0$) to rhombohedral ($x = 0.2$ and 0.4). Moreover, it regularly increased the bandgap energy from 1.34 eV (when $x = 0$) to 2.07 eV (when $x = 1$) and the valence band maximum systematically varied from −4.91 eV ($x = 0$) to −5.50 eV ($x = 1$). Thus, they demonstrated that with this strategy, they were able to tune the electronic and optical parameters of the perovskite through fine variation of the crystal structure. Their champion device with HEAI 40% ($x = 0.4$) showed the best PCE of 3.7% for a fresh cell and 3.9% for the device stored in a glovebox for 340 h.

Other A-site cations have been studied in the literature to increase the durability of lead-free Sn-HPSCs, because the rate of Sn(II) oxidation in $MASnI_3$ is higher than in $FASnI_3$[25]. In 2018,

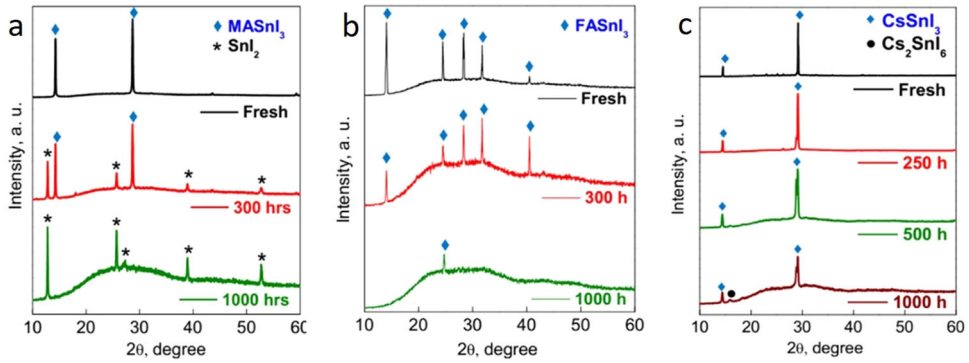

Fig. 2 Effects of temperature exposure with time on different perovskite compositions. Evolution of the structure with time followed by the XRD patterns of **a** $MASnI_3$, **b** $FASnI_3$, and **c** $CsSnI_3$, after thermal annealing at ~90 °C. (Fig. 2 adapted with permission from ref. [19], Copyright 2019 ACS Publication).

Jokar et al. investigated the dopant effect of ethylenediammonium diiodide ($EDAI_2$) with butylammonium iodide in the Sn-HPSCs[26]. In the presence of $EDAI_2$, the tin vacancies inside the $FASnI_3$ crystals were occupied decreasing the background carrier densities that resulted in longer lifetimes of the charge carriers. Thereby, they concluded that the crystal growth was slowed down permitting the formation of pinhole-free films[26, 27]. Jokar et al. mixed as well the organic cation guanidinium ($CH_6N_3^+$, GA) with FAI in increasing proportions and added 1% $EDAI_2$ and 10% SnF_2 as dopants to improve the device performance of the Sn-HPSCs[28]. They chose GA^+ because of its slightly bigger size than FA^+ and ability to co-crystallise with it. The best device of this 3D-structured series was $FA_{0.78}GA_{0.2}SnI_3$ which showed PCEs increasing from 8.5%, when freshly prepared, to 9.6% after storage in a glovebox for 2000 h. Moreover, the unencapsulated device demonstrated good stability in the air (with relative humidity, RH, of 20%) for 1 week and retained 80% of its initial efficiency after 100 h in a more rigorous condition (RH 60%) (Table 1). Later, the same group incorporated azetidinium (AZ) into the $FASnI_3$ perovskite precursor, reporting a record PCE of 9.6% with the $AZ_{0.15}FA_{0.85}SnI_3$ structure[29]. Furthermore, the best encapsulated device retained 90% of initial efficiency after 360 h (Table 1).

A different approach consists in the use of Cs(I) because it tends to enhance the long-term stability of mixed-cation Sn-HPSCs[30]. The addition of Cs(I) contracts the crystal lattice and permits the deposition of denser films that enhance the stability of Sn-HPSCs in ambient conditions[31]. Liu et al. combined organic (FA^+) and alkali metal (Cs^+) cations to study its effect on device performance and long-term stability[32]. Moreover, they added dopants like ethylenediammonium diiodide ($EDAI_2$), SnF_2, and $SnCl_2$ to the perovskite precursor to obtain a pinhole-free and passivated perovskite surface. Despite the hygroscopic nature of $SnCl_2$, the Sn-3X ($CsFASnI_3$-$EDAI_2$ with 10 mol% of SnF_2 and 20 mol% of $SnCl_2$) structure gave rise to films with a lower concentration of defects and attenuated water and oxygen channels that improved the long-term stability of the Sn-HPSCs. After addition of 20% $SnCl_2$, the encapsulated champion device retained over 95% of its initial PCE in a N_2-filled glove box after operation at the maximum power point (MPP) under continuous 1 sun illumination for 1000 h (Fig. 3a, Table 1).

2D/3D and quasi-2D perovskites. The dimensionality of the perovskite structure can be effectively reduced from 3D to 2D/3D perovskite mixtures or 2D replacing the A-site cation by bulky organic molecules as mentioned in "Compositional engineering of the lead-free tin-based perovskite". These large molecules have many advantages such as providing higher open-circuit voltage due to the larger band gap, improving film quality via slowing down the crystallisation rate, or having more tuneable structures that allow higher flexibility in the chemical structures in comparison to the 3D perovskites[33, 34]. Above all, they mainly passivate surface defects preventing the incorporation of oxygen and water due to the enhancement of the steric hindrance on the surface of the perovskites[13, 35]. Recently, low-dimensional perovskite structures have received more attention due to their higher thermodynamic stability in comparison to 3D structures[36]. It has been reported that low-dimensional perovskites show reduced background carrier density in comparison to pure 3D $FASnI_3$ perovskite[37]. To understand the crystallisation process of low-dimensional tin perovskite, Qiu et al. introduced a mixture of organic cations [*n*-butylamine (BA) and phenylethylamine (PEA)] as spacers into the $FASnI_3$-based perovskite precursor[38]. These mixed organic cations acted as 2D intermediate phase inhibitors, resulting in lower bulk defects and surface traps. The 2D intermediate phase causes uneven nucleation, disordered orientation and promotes parallel growth orientation to the substrate. Thus, the inhibition of this phase lead to PCE values of 8.82%. However, the use of bulky organic cations alone does not sufficiently improve the long-term stability of Sn-HPSCs, as reported in the literature. Li et al. reported low-dimensional all-inorganic $CsSnBrI_2$-based Sn-HPSCs to investigate the complete unencapsulated devices in ambient air (RH 60–70%)[39]. Devices based on $CsSnBrI_2$-PS (PS indicating the presence of PEAI and $Sn(SCN)_2$), consisting of 15% PEAI and 7.5% $Sn(SCN)_2$ led to a champion PCE of 5.01%, and the unencapsulated best cell retained 78% of its initial efficiency under ambient air for 4 h (Table 1).

Although inorganic cations form fewer decomposition products, mixing organic cations with bulky organic cations can lower trap density in the bulk and improve the quality of Sn-HPs films[40, 41]. More recently, Yu et al. incorporated the fluorinated bulky organic cation FPEABr to the $FASnI_3$ perovskite precursor to modulate the microstructure of the 2D/3D heterogeneous Sn-HPs light absorber[12]. The device's performance was improved with this unique microstructure which suppressed the oxidation of Sn and lowered the density of defects. They compared the performance of four compositions of Sn-HPSCs with varying ratios of FPEABr:FAI. Herein, while a pure 3D $FASnI_3$-based device reached PCE of 9.38%, 2D/3D Sn-HP with 10% FPEABr showed a champion efficiency of 14.81% (Fig. 3b). In the 2D/3D Sn-HP photoactive layer, the 2D phase embraces 3D grains and is mainly located at the top and bottom surfaces and grain boundaries. Their study purposedly chose a fluorinated compound to block the water penetration and offer a reduced atmosphere for vulnerable 3D $FASnI_3$. Thus, they demonstrated that the encapsulated 2D/3D Sn-HPSCs retained 80% of the initial value for 432 h when exposed to air, while the encapsulated control 3D devices maintained it only for 265 h (Fig. 3c, Table 1).

Table 1 Summary of the stability attained by Sn-HPSCs made with different perovskite compositions.

Perovskite composition	Structure, additives	Device architecture	Ageing condition and illumination	Tracking time (h)	Load	Champion PCE (%)	PCE retained (%)	Year
$FAMASnI_3$	3D, SnF_2	ITO/PEDOT:PSS/ $FAMASnI_3$/C_{60}/ BCP/Ag	Unencapsulated, Oriel 300 W solar simulator	400	Shelf stability in N_2	8.12	80[23]	2017
$FASnI_3$	3D, SnF_2 and 5-AVAI	ITO/PEDOT:PSS/ $FASnI_3$/PCBM/ BCP/Ag	Encapsulated in 50% RH, 1 sun irradiation; <420 nm UV cut filter	100	MPP tracking	7.00	100[133]	2018
$FASnI_3$	2D-quasi-2D-3D, SnF_2, NH_4SCN and PEAI	ITO/NiO_x/$FASnI_3$/ PCBM/BCP/Ag	Unencapsulated in N_2, 100 mW/cm^2 (1 sun)	300	MPP tracking	9.41	90[10]	2018
$FAGASnI_3$	3D, $EDAI_2$, SnF_2	ITO/PEDOT:PSS/ $FAGASnI_3$/C_{60}/ BCP/Ag	Unencapsulated in 60% RH, 100 mW/cm^2 (1 sun)	100	Shelf stability in air	9.60	80[28]	2019
$FASnI_3$	3D, SnF_2	ITO/PEDOT:PSS/ $FASnI_3$/PEABr/ PCBM/BCP/Al	In ambient air, AM 1.5 G	350	Light soaking	7.86	80[43]	2019
$FASnI_3$	3D, SnF_2 and FBH	ITO/(PEG)-PEDOT:PSS/ $FASnI_3$/C_{60}/BCP/ Ag	Encapsulated in 20% RH, Class AAA solar Simulator	600	MPP tracking	9.47	93[134]	2020
$FASnI_3$	2D/3D, SnF_2 and PAI	ITO/PEDOT:PSS/ $FASnI_3$/C_{60}/BCP/ Ag	Unencapsulated in N_2, Class AAA solar simulator; <420 nm UV cut filter	1000	MPP tracking	11.22	95[11]	2020
$CsFASnI_3$	2D/3D, SnF_2, $SnCl_2$ and $EDAI_2$	ITO/PEDOT:PSS/ $CsFASnI_3$/PCBM/ BCP/Ag	Encapsulated in ambient air, Class AAA solar simulator	1000	MPP tracking	10.79	95[32]	2020
$AZFASnI_3$	3D, $EDAI_2$, SnF_2	ITO/PEDOT:PSS/ $AZFASnI_3$/C_{60}/ BCP/Ag	Unencapsulated in ~55% RH, 100 mW/cm^2 (1 sun)	360	Shelf stability in air	9.60	90[29]	2021
$GAFASnI_3$	3D, $EDAI_2$, SnF_2	ITO/ PEDOT:PSS/ $GAFASnI_3$/ PHSCN/ C_{60}/BCP/ Ag	100 mW/cm^2 (1 sun)	3000	Shelf stability in N_2	13.50	92[46]	2021
$FASnI_3$	3D, SnF_2, $SnBr_2$, and PHCl-0.1Br	ITO/PEDOT:PSS/ $FASnI_3$/C_{60}/BCP/ Ag	Unencapsulated, solar simulator (940043 A),	330	Shelf stability in N_2	13.40	82[91]	2021
$CsSnBrI_2$	2D/3D, PEAI, $(SCN)_2$	ITO/PEDOT:PSS/ $CsSnBrI_2$/PCBM/ BCP/Ag	Unencapsulated, RT, RH = 60–70%, under an atmosphere	4	PCE tracking	5.01	77[39]	2021
$FASnI_3$	2D/3D, SnF_2, FPEABr	ITO/PEDOT:PSS/ $FASnI_3$/ICBA/BCP/ Al	Encapsulated in air, RH = 75%, 20 °C	432	PCE tracking	14.81	80[12]	2021
$FAMASnI_2Br$	Sn^0 powder, SnF_2, PEAI	ITO/PEDOT:PSS/ $FAMASnI_2Br$/ CF_3PEAI/PCBM/ BCP/Ag	Unencapsulated in air 15% RH, 100 mW/cm^2 (1 sun)	150	Shelf stability in air	10.35	70[45]	2022
$FASnI_3$	3D, $NaBH_4$ and DipI	ITO/PEDOT:PSS/ $FASnI_3$/C_{60}/BCP/ Ag	Unencapsulated in N_2, Xenon lamp	1300	MPP tracking	10.20	96[96]	2022

The additives employed and resulting structure are also indicated. *MPP* maximum power point, *PCE* power conversion efficiency, *RT* room temperature, *RH* relative. humidity.

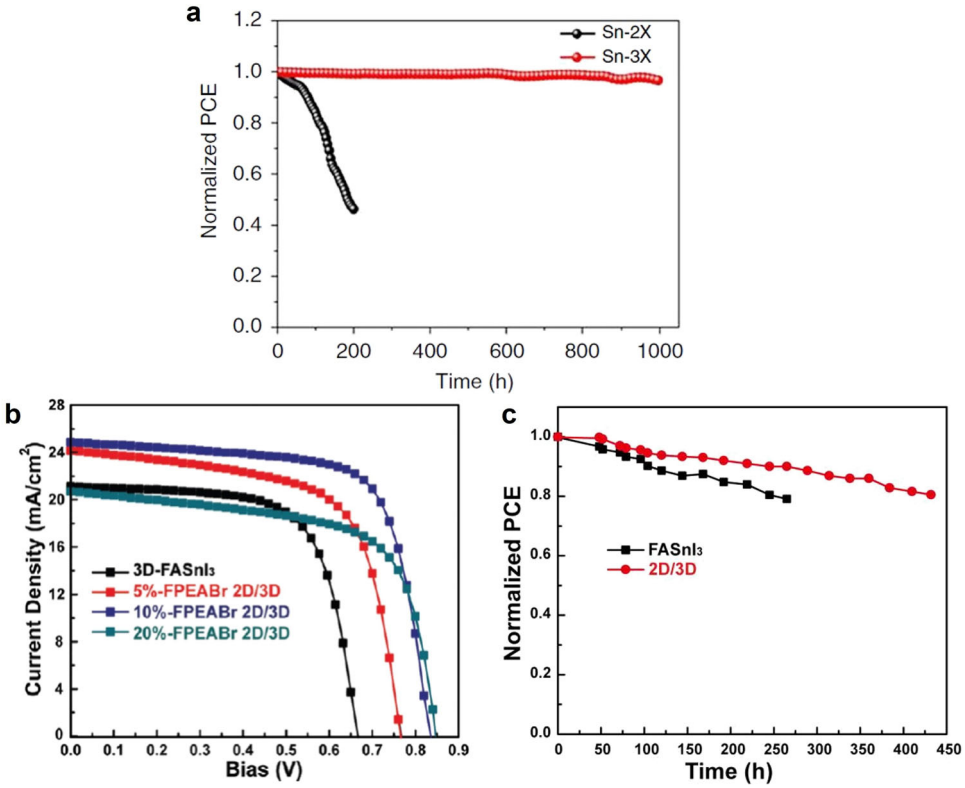

Fig. 3 Stability of 3D and 2D/3D Sn-HPSCs prepared with various additives. a The maximum power point (MPP) tracking of the unencapsulated devices with (Sn-3X) and without (Sn-2X) $SnCl_2$ addition. **b** Best current density–voltage (*J*–*V*) curves for pure 3D and 2D/3D Sn-HPSCs with different FPEABr content. **c** Normalised PCE evolution of the 3D $FASnI_3$ and 2D/3D perovskite-based encapsulated devices in air (Fig. 3a adapted with permission from ref. [32], Copyright 2020 Springer Nature. Fig 3b, c adapted with permission from ref. [12]., Copyright 2021 Wiley).

Materials with the ability to form lower dimensional perovskites have also been employed for the surface treatment of the photoactive films. Though many different molecules have been screened[42], PEA salts have become the most popular surface modifiers. Liao et al. deposited a very thin layer of PEABr on top of the perovskite film forming low dimensional material[43]. The improved quality of the surface led to optimised band alignment and lower defect density, enhancing the device efficiency and its stability to oxidation, retaining 80% of the initial performance after 350 h of light soaking. Choi et al. used instead the iodide salt, PEAI, also reporting a higher stability against Sn(II) oxidation[44]. Moreover, PEA^+ molecules can be functionalised to tune their properties. In this regard, Chen et al. deposited a trifluoromethyl derivative of PEA on the perovskite surface to increase its hydrophobicity and air stability in devices with efficiencies over 10%[45]. Furthermore, Jokar et al. applied phenylhydrazinium thiocyanate (PHSCN) on a hybrid mixed cationic tin perovskite film to improve the device's stability[46]. The best device retained 92% of the initial PCE after storing for 3000 h (Table 1).

The role of the device structure

Architecture

Mesoporous configuration (n-i-p). The so-called mesoporous n-i-p architecture is one of the most popular ones reported for tin and lead PSCs (Fig. 4a). The electron selective layer (ESL) in this architecture comprises a compact titanium dioxide (TiO_2) layer, which acts as ESL, and a mesoporous TiO_2 layer that acts as a scaffold for the photoactive layer. On the other side, the hole selective layer (HSL) consists mainly of 2,2′,7,7′-tetrakis[N,N-di(4-methoxyphenyl)amino]−9,9′-spirobifluorene (Spiro-OMeTAD) or poly[bis(4-phenyl)(2,4,6-trimethylphenyl)amine (PTAA). Despite its popularity, this structure has several drawbacks for obtaining highly efficient and long-term stable Sn-HPSCs; for example, TiO_2 can contain oxygen vacancies, which oxidise Sn(II) to Sn(IV). In addition, the p-type dopants applied on the TiO_2 are hygroscopic (such as lithium and cobalt salts) and promote the absorption of moisture or oxidation of Sn(II)[47].

Planar architecture (n-i-p vs p-i-n). The planar structure is made by a multilayer stack where each layer has a specific role. In contrast to the mesoporous architecture, the layers are planar and deposited step-by-step, by evaporation or solution techniques, onto the previous layer. In addition, the charge selective layers can be deposited onto the substrate or on top of the photoactive layer and below the metallic electrode. The nomenclature of n-i-p or p-i-n, therefore, indicates the position of the charge transport layers from the substrate to the upper electrode.

In the case of Sn-HPSCs, the devices show better performance when prepared with the inverted planar structure (p-i-n, Fig. 4b) than with the regular one (n-i-p, Fig. 4c), what has motivated the researchers to apply this structure, especially in the two last years[48]. As aforesaid, due to the drawbacks of TiO_2 and Spiro-OMeTAD as charge selective layers, other materials have been tested in planar configurations. One of the most efficient combinations in an inverted structure is achieved with phenyl-C61-butyric acid methyl ester (PCBM) as ESL and poly(3,4-ethylenedioxythiophene):polystyrene sulfonate (PEDOT:PSS) as HSL. This composition shows lower conduction and valence bands offsets than the regular structure prepared with TiO_2 and Spiro-OMeTAD, which results in the decrease of the over-potential at the interface and increase the transport and extraction of the charges[49–51]. In this sense, the fullerenes in an inverted structure, such as C60 and PCBM, passivate the surface of the perovskite film improving the open-circuit voltage (V_{OC}).

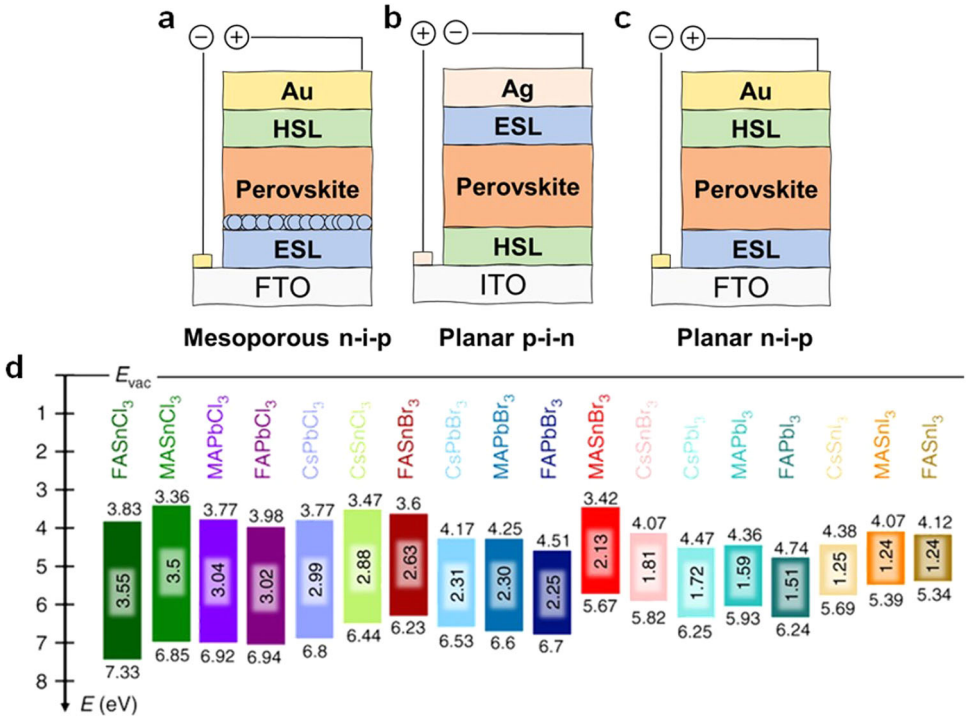

Fig. 4 Illustration of the different types of architectures of the perovskite devices and energy level diagrams of different compositions of perovskites. PSCs with **a** mesoporous n-i-p **b** planar p-i-n and **c** planar n-i-p device structures. **d** Schematic band diagrams of tin perovskites compared to lead perovskites. (Fig. 4 a–c adapted with permission from ref. [135]. Figure 4d reprinted with permission from ref. [53], Copyright 2019 Springer Nature).

Finally, the application of 2,9-dimethyl-4,7-diphenyl-1,10-phenanthroline (BCP) as a hole blocking layer reduces charge recombination and enhances the performance[52].

Charge selective layers. Charge selective layers (CSLs) are responsible for the collection of the photogenerated charges towards the electrodes. One of the reasons of the lower efficiency of Sn-HPSCs versus Pb-HPSCs is the high voltage (V_{OC}) loss (between 0.4 and 0.5 eV) due to the oxidation potential of Sn(II) and the misalignment between the energy bands of the photoactive material and the CSLs. Apart from Sn(II) oxidation, the huge V_{OC} deficit in Sn-HPs is the most significant impediment for developing highly efficient Sn-HPSCs. Sn-HPs have shallower conduction and valence band maximum values than lead-based halide perovskites (Pb-HPs), creating an energy barrier at the perovskite/CSL interface (Fig. 4d)[53]. Therefore, charge transfer and extraction decrease resulting in massive voltage losses. In the next section, we describe recent research in different CSLs, and the strategies developed to minimise the voltage loss.

Organic CSLs (ESLs and HSLs). Most of the CSLs applied in Sn-HPSCs are organic due to their versatility and ease of tailoring; however, they still suffer from the energy band mismatch. Tremendous research effort has been devoted to tune the energy level offsets of the organic molecules to match the photoactive material. Still, the most used organic CSLs in Sn-HPSCs are the commercial hole transporting materials Spiro-OMeTAD, PTAA, and PEDOT:PSS.

Spiro-OMeTAD was the first HSL adopted by the tin perovskite community in a mesoporous architecture. However, the highest reported efficiencies ranged between 5 and 6%[54–58]. Recently, Mahmoudi et al. applied Spiro-OMeTAD as HSL in a regular mesoporous structure and achieved a PCE of 7.7% using reduced graphene oxide sheets and tin quantum dots to suppress the Sn (II) oxidation[59].

On the other hand, with the best efficiencies approaching 7%, PTAA has shown relatively better results than Spiro-OMeTAD, and thus has been more frequently reported in the literature. Hu et al. used PTAA as HSL in n-i-p mesoporous architecture and achieved a PCE of 9.06%, the highest reported value for n-i-p devices[60]. This study proved that PTAA could be utilised as HSL in high-efficiency Sn-HPSCs, providing good alignment with the energy bands of the photoactive material.

Regarding, PEDOT:PSS, it became the most adopted organic HSL in Sn-HPSCs[61]. This is attributed to the functional properties of PEDOT:PSS, such as good wettability, better alignment of the energy levels, and easy processability. Therefore, many researchers has worked to tune the electronic and structural properties of PEDOT:PSS to maximise the performance of Sn-HPSCs[62–65]. Recently, Shih et al., used the water-soluble zwitterion sulfamic acid to enhance the hole extraction and transportation properties of PEDOT:PSS by increasing its mobility and conductivity[66]. As a result, the front orbitals of the deposited perovskite film at the interface were modified, facilitating the charge transfer and increasing the energy band alignment. The best-treated samples achieved a PCE of 10.5%. Moreover, the best samples showed high stability upon storage in the glovebox and retained 95% of their initial efficiency after 2000 h. This study reveals the importance of the interface design and treatment for both efficiency and stability[66].

Inorganic CSLs. Inorganic materials are generally more robust than organic molecules due to their chemical stability and resistivity[67], and were widely used in the early reports about Sn-HPSCs. Examples of CSLs are mesoporous titanium dioxide (m-TiO_2)[60], mesoporous aluminium oxide (m-Al_2O_3)[59], and compact niobium oxide (c-Nb_2O_5)[68] as electron CSLs (ESLs) and NiO_x[69], Cu-NiO_x[70], and CuSCN[71] as hole CSLs (HSLs). In 2020, Li et al., compared the shelf-stability of PEDOT:PSS and NiO_x in Sn-HPSCs stored in a N_2-filled glovebox[69]. NiO_x-based devices

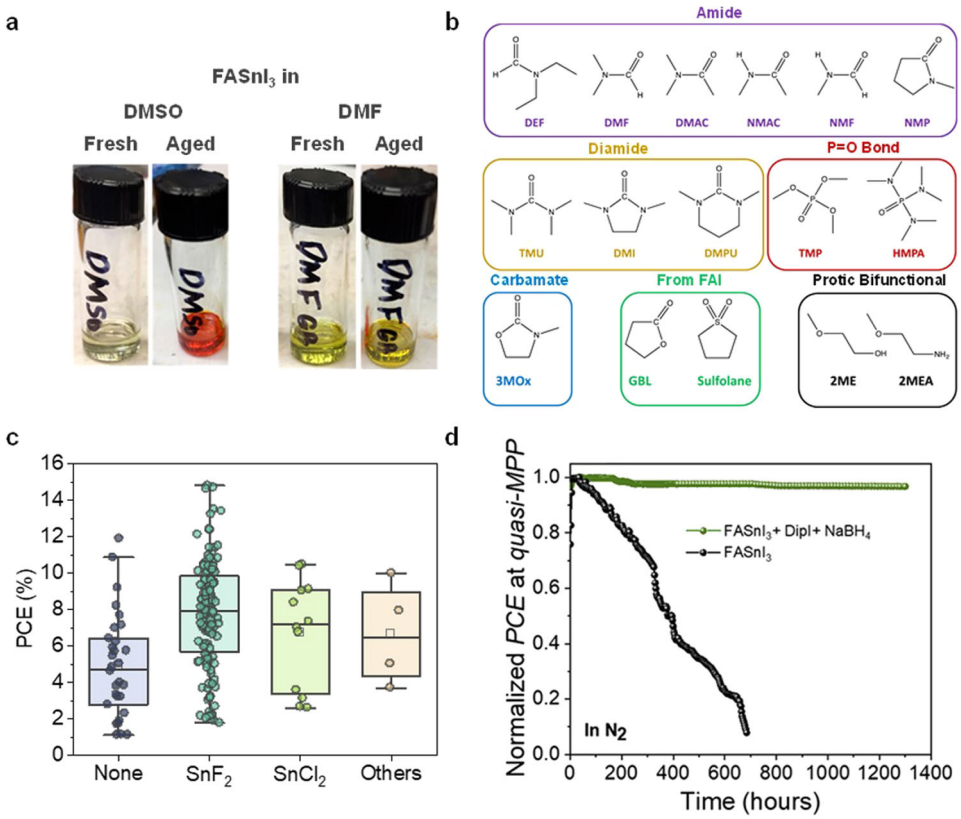

Fig. 5 Effects of solvents and additives on the photovoltaic performance and stability of Sn-HPSCs. a Fresh and aged (120 °C for 5 h) $FASnI_3$ solutions in DMSO and DMF. The colour change to red for aged DMSO solution suggests the presence of oxidised Sn species. **b** List of solvents capable of forming $FASnI_3$ solutions. **c** PCE distribution of reported devices in literature containing different SnX_2 additives. **d** Normalised PCE evolution at MPP in N_2 atmosphere of devices based on $FASnI_3$ perovskite with and without DipI + $NaBH_4$ antioxidant additive strategy. (Fig. 5a adapted with permission from ref. [6], Copyright 2020 ACS Publications. Figure 5b adapted with permission from ref. [77], Copyright 2021 ACS Publications. Fig 5d reprinted with permission from ref. [96]., Copyright 2022 Elsevier).

showed higher efficiency and stability than PEDOT:PSS-based ones, demonstrating the potential of inorganic HSLs for the preparation of long-term stable Sn-HPSCs. Following the same trend, Wang et al., reported an air-stable Sn-HPSC containing NiO_x as HSL[72]. The improved stability in air of the device could be attributed to the addition of gallic acid to the photoactive material; however, the presence of NiO_x proved that it is also air-stable and degradation resistant and assured its suitability as HSL for highly stable Sn-HPSCs.

Researchers recently shifted to the inverted planar structure based on organic ESLs, mainly C60 and fullerene derivatives. Meanwhile, a few reports showed the potential of some other inorganic ESLs such as Nb_2O_5 and SnO_2 for highly efficient Sn-HPSCs[68]. However, to the best of our knowledge, no comprehensive study has revealed the effect of the different inorganic ESLs on the efficiency or long-term stability of Sn-HPSCs.

Metallic electrodes. The effect of the top metal electrode on the efficiency and stability of Sn-HPSCs have not been fully explored. In 2021 Wijesskara et al. replaced the traditional Ag/BCP electrode by Cu/BCP in an unencapsulated Sn-HPSCs. The Cu electrode remarkably stabilised the device in comparison to the Ag electrode against degradation in ambient air and light soaking. This work highlights the importance of properly combining metal electrodes and HSLs to increase the long-term stability for Sn-HPSCs[73].

Strategies to increase stability

Solvent engineering. In addition to the sources mentioned above, dimethyl sulfoxide (DMSO) was also found to induce the oxidation of Sn(II) in Sn-HP solutions (Fig. 5a). Saidaminov et al. reported in 2020 that the redox reaction between these two compounds was promoted at high temperatures[6]. Our laboratory later investigated the particularities of the reaction, proposing a reaction mechanism by direct identification of Sn(IV) with NMR[7]. The solution contents affect the Sn(II) oxidation, being promoted in acidic conditions and reduced in the presence of SnF_2 additive. Considering that almost every processing protocols involve DMSO-based solvent systems, this reaction could have been hampering critically the development of Sn-HPs, also regarding their particularly low defect tolerance[17, 74]. However, the extent of this oxidation during the processing and the actual implications on device performance are still open to discussion[75].

Despite the evidence supporting the detrimental effect of DMSO, the reported attempts to replace it are still scarce. First reports of Sn-HPs fabrication involved using pure *N*,*N*-dimethylformamide (DMF)[54, 56]. Due to its low binding strength to the precursors, this solvent could not control the rapid crystallisation of Sn-HPs, thus leading to low-quality films. In fact, after applying DMSO in the inks, the field started to quickly develop, thanks to the formation of SnI_2·xDMSO intermediate species improving the nucleation and crystal growth processes[76]. The dependence that a controlled crystallisation currently has on DMSO may be hindering the development of new solvent systems to process high-quality Sn-HP thin films. To address this

problem, our group screened over 80 solvents to investigate the parameters required to form stable DMSO-free $FASnI_3$ solutions (Fig. 5b)[77]. From the 12 solvents that were found suitable, a mixture of *N*,*N*-diethylformamide (DEF) and *N*,*N*′-dimethylpropyleneurea (DMPU) led to excellent thin films and devices exceeding the performance of those from DMSO systems without the use of any additive. Binary solvent systems with different volatility and binding strength to Sn(II) are useful for modulating the kinetics of thin-film formation and offer a possibility for the future development of oxidant-free Sn-HP precursor solutions.

SnX_2-based additives. A practical and widely used strategy to improve the quality and stability of Sn-HP thin films is using additives with the SnX_2 (X = F, Cl, Br) structure (Fig. 5c). The most significant one is SnF_2, currently used in almost every reported device. First presented by Kumar et al. in 2014[78], the application of this additive was a crucial step in the community for improving the low performance and reproducibility of Sn-HP materials[79, 80]. Several scientists systematically reported its beneficial effects, particularly on increasing the stability of Sn-HPs to oxidation[49, 81, 82]. In 2021, our group proved the importance of fluoride anions in SnF_2 for stability[83]. The hard Lewis basicity of fluoride in comparison to iodide promotes the complexation of all Sn(IV) in the form of SnF_4, preventing its incorporation in the perovskite film, and also affects the colloidal nature of the perovskite precursors in solution, promoting more homogeneous nucleation. Therefore, the chemical role of fluoride in solution and the excess Sn(II) being introduced, which reduces Sn vacancies[84], makes SnF_2 an excellent versatile additive.

$SnCl_2$ is also a good additive used by different research groups that can positively affect the perovskite thin-film quality and its oxidation resistance[85, 86]. Chloride, being a harder Lewis base than iodide, may act through a similar mechanism to SnF_2, potentially making both additives interchangeable to a certain extent. This same behaviour may be shared by other SnX_2 additives also successfully implemented to enhance the stability of Sn-HPs. These include $SnAc_2$ (Ac = acetate), $SnAcac_2$ (Acac = Acetylacetonate) and $Sn(SCN)_2$[87–89]. In fact, other non-Sn-based additives bearing these same counter-anions have also shown benefits on device performance, highlighting the potential of bifunctional additives for versatile applications in precursor solutions[10, 90].

Non-halide reducing agents. A direct strategy to tackle the problems derived from oxidised species is introducing reducing agents. Most of them involve using acidic species, such as hydrazinium[91–93], hypophosphorous acid[94], formic acid[95], gallic acid[72], or potassium salt of hydroquinone sulfonic acid[86]. In particular, Wang et al. achieved efficiencies of over 13%, introducing an unprecedented healing behaviour after exposing to air the Sn-HP films containing phenylhydrazinium derivatives[91, 93]. Recently, Sanchez-Diaz et al. employed sodium borohydride ($NaBH_4$) in combination with dipropylammonium iodide (Dipl) to achieve $FASnI_3$-based devices with over 1300 h of operational stability (Fig. 5d, Table 1)[96]. This result represents a milestone demonstrating that Sn-HPSCs hold potential for long-term stability, regardless of their redox behaviour.

However, the transferability from the lab to the lab of protocols using the same specific reducing species remains a challenge. The one showing the highest reproducibility, considering the number of laboratories that have successfully applied, is metallic Sn powder, which can undergo a comproportionating reaction with Sn(IV) species[42, 97, 98]. To further enhance the effectiveness and applicability of antioxidant strategies, future studies should focus on understanding the implications and compatibility of additives with specific perovskite structures.

Environmental factors

Environmental factors, such as humidity, oxygen, temperature, and light, significantly affect the stability of Sn-HPSCs by inducing a phase transition, trap states, or crystal decomposition due to the significant presence of grain boundaries in the polycrystalline thin films[33, 47]. Insight into the degradation mechanisms by environmental factors is essential for proposing strategies to improve the stability of Sn-HPs and the device's performance.

Humidity. Similar to the case of Pb-HPSCs, Sn-HPSCs are also sensitive to humidity, owing to the hygroscopic nature of organic MA^+ and FA^+ cations. Ahmad et al. proposed the possible decomposition pathway of MA^+ cation in Sn-HPs in the presence of water[99]. In case of sufficient water, Sn-HPs firstly decomposed into MAI and HI. MAI is further deprotonated by water to form volatile *sym*-triazine and NH_4I until wholly decomposed. In addition to the decomposition of organic cations, H_2O prefers to form the H-I bond, which weakens the Sn-I bond on the $MASnI_3$ surface, affecting the stability of the surface[100]. Sn-HPs made with inorganic cations also suffer the issue of water instability, as investigated by Yang et al. investigated in $CsSnI_3$ by density functional theory (DFT) calculations[101]. The results showed that the black and photoactive phase γ-$CsSnI_3$ is hydrophilic-like, and H_2O tends to adsorb at the hollow sites on the (001) surface, rendering the structure deformation towards a non-photoactive phase.

Oxygen. Oxygen significantly affects the stability of Sn-HPs, owing to the tendency of Sn(II) to oxidise towards the stable Sn(IV) state. This introduces a high density of Sn vacancies, which will further lead to serious p-type doping of the material with a limitation of carrier diffusion length[82]. Haque et al. investigated the degradation mechanism of $(PEA)_{0.2}(FA)_{0.8}SnI_3$ perovskite under ambient environmental conditions[14]. They showed that oxygen can induce the degradation of Sn-HPs towards SnI_4. Moreover, SnI_4 in the film readily evolves into I_2 with the assistance of moisture, which will further accelerate the degradation of perovskite material into more SnI_4 (Fig. 6a). A DFT calculation also indicated that O_2 can be spontaneously adsorbed on the $FASnI_3$ surface and induce iodide vacancies[102]. In particular, under light exposure, the photogenerated electrons could further promote the O_2 adsorption on the surface and promote the formation of iodide vacancies. Additionally, structural changes can also be observed by weakening FA^+—I^- interactions and forming H_2O, OOH^-, and H_2O_2 on both surface and subsurface, further leading to the instability and final degradation of $FASnI_3$.

Temperature. The effect of temperature on the stability of Sn-HPs is mainly seen in the induction of phase transitions. In general, a more symmetric structure with black and photoactive phases can be obtained upon increasing the temperature, such as $CsSnI_3$ with black cubic (B-α) at 227 °C, tetragonal (B-β) at 107 °C, and orthorhombic (B-γ) at 27 °C (Fig. 6b). However, under room temperature, photoactive B-γ-$CsSnI_3$ can be rapidly degraded into the yellow (Y) phase, which further transforms to the photo-inactive Cs_2SnI_6 with exposure to air due to the oxidation of Sn(II) to Sn(IV)[47]. Moreover, the organic MA and FA cations in Sn-HPs decompose at 200 °C, showing lower thermal stability in comparison to Cs-based Sn-HPs, that with a melting point as high as 451 °C due to the strong covalent/ionic interaction between Cs^+ and halogen anions, facilitates the formation

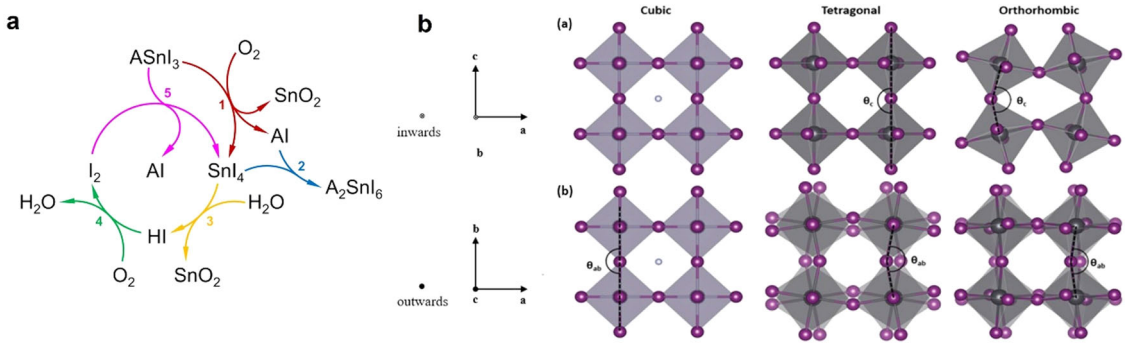

Fig. 6 Impact of the environmental factor impact on Sn-HPs. a Proposed cyclic degradation mechanism of tin-based perovskites under O_2 and H_2O **b** Cubic-α, tetragonal-β, and orthorhombic-γ structure of black-photoactive phases (Fig. 6a reprinted with permission from ref. [14], Copyright 2021 Springer Nature. Fig 6b reprinted with permission from ref. [47], Copyright 2021 Wiley-VCH GmbH).

of the $[SnI_6]^{4-}$ octahedron. Thus, the free energy is reduced along with the enhancement of the thermodynamic stability of the crystal structure[103, 104].

Light exposure. Analogous to Pb-HPs, light-oxygen-induced degradation is also a significant environmental pathway to decompose Sn-HPs. Jin et al. applied DFT calculations to reveal that light illumination and oxygen absorption on the $FASnI_3$ surface greatly promoted the formation of iodide vacancies. Significantly, the photogenerated electrons can form superoxides when interacting with O_2 under light exposure, which causes the degradation of $FASnI_3$[102]. In addition, as for the Sn-HPSCs with mesoporous TiO_2 structure, UV-light can further accelerate the degradation of perovskite due to the photocatalytic effect of TiO_2 in the presence of UV, which is similar to what is reported for Pb-HPSCs[105].

Losses in efficiency due to intrinsic factors

The losses in the performance in Sn-HPSCs still arise even when ruling out external sources of degradation. These reactions are due to the intrinsic characteristics of the device and the constituent materials, such as carrier trapping-detrapping, grain boundaries, the polarisation of the metallic electrodes, ion migration in the photoactive layer, the ferroelectric effect of the photoactive layer, and halide segregation in mixed halide systems[106–110].

The fast and more popular technique to determine the efficiency of the devices is the measurement of the variation of the current density and voltage under light illumination, the so-called *J–V* curve. However, as simple as it may seem, changes in the scan conditions (i.e., scan rate, scan speed, etc) during the measurement generate hysteresis of different magnitudes in the *J–V* curve, being this still a matter of concern when comparing the efficiencies reported in the literature. In fact, the main causes for the observation of hysteresis are due to the materials forming the device, such as the phase discontinuity of the photoactive film, inactivation caused by defects, the kinetics in the extraction of charge carriers at the interface, and the quality of the photoactive layer[106, 111]. But despite the influence of the materials, the scan specifications are at the end critical parameters to determine the PCE of the devices. A higher open-circuit voltage values are obtained when the scan is done from open circuit to short circuit of PSCs, instead of from the short circuit to the open circuit at *J–V* measurement. Also, the *J–V* hysteresis seems very small for a higher scan rate (~200 mV/s), the PSC performances are precise, and the hysteresis index (HI) is also close to zero. Moreover, the hysteresis increases with a higher scan rate with higher HI[109]. In a few cases, the measurement of the PSCs done with a slow scan rate result in lower values of hysteresis[112], which is due to the non-steady-state capacitive current influence shown in interval times. However, the application of different time measurements could not be the most appropriate way to report device performance[113]. Nevertheless, to minimise the HI value requires either stabilisation of the power output or determination of the maximum power in the *J–V* curve. The variations that can be observed in the hysteresis of the *J-V* curve under different scanning conditions such as switching the scanning direction, illumination conditions, scan rate, or the effect of temperature are shown in Fig. 7a-c[114, 115].

Ion migration is another determining factor in the observation of hysteresis. The migration is associated to a change in the interfacial fields and barriers, which leads to charge recombination by the accumulation of ions at the interface[116]. By the effect of exposure to external light, thermal drift, or voltage bias, the migrated ions across the bulk perovskite layer can induce an electric field which affects the charge collection efficiency leading to poor stability. During the forward scan, there is a reduced recombination between photogenerated charges at the interfaces, due to the build-up of electrical fields that contribute to the efficient collection of diffusive currents. Therefore, the combination of low interfacial recombination and high photogenerated carrier populations at forward bias will result in low hysteresis[116]. Ion migration is also facilitated by interfacial charge distribution and lattice defects including vacancies and interstitials, which affects the photoelectronic properties and long-term stabilities[116]. During the preparation of perovskite films, it is common to generate vacancies in the perovskite structure, and these defects can enhance ion migration (Fig. 7e), resulting in low PCE and even causing device failure during operation. For example, a reaction between the hole-transport layer and the migrating iodine ions can reduce the conductivity in the HSL. The migrated ion build-up a local electric field at the Sn-HPs interface, leading to the deterioration of the PSCs and deprotonation of the organic cations[117]. In turn, ions migrated from the conductive contacts (HSL or ESL) to the perovskite layer can create shunt pathways for electrons leading to the short-circuiting of PSCs, because of hybrid perovskite have different diffusion coefficient and low activation barrier for MA^+/FA^+ and I^- ion[99, 116]. The addition of organic polymers (such as poly vinyl alcohol – PVA) to the $FASnI_3$ increases the hydrogen bonding and interactions with iodine ($O-H\cdots I^-$) at the grain boundary. This interaction hinders the diffusion of iodide ions, restricts the formation of iodine vacancies (by increasing the atomic ratio of iodine ion (I:Sn) in the surface of $FASnI_3$) and decreases the ionic conductivity (σ_{ion})[99, 116]. Moreover, the polymer addition favours the formation of nucleation sites in the Sn-HP, reducing the trap states and slowing down the crystal growth[99].

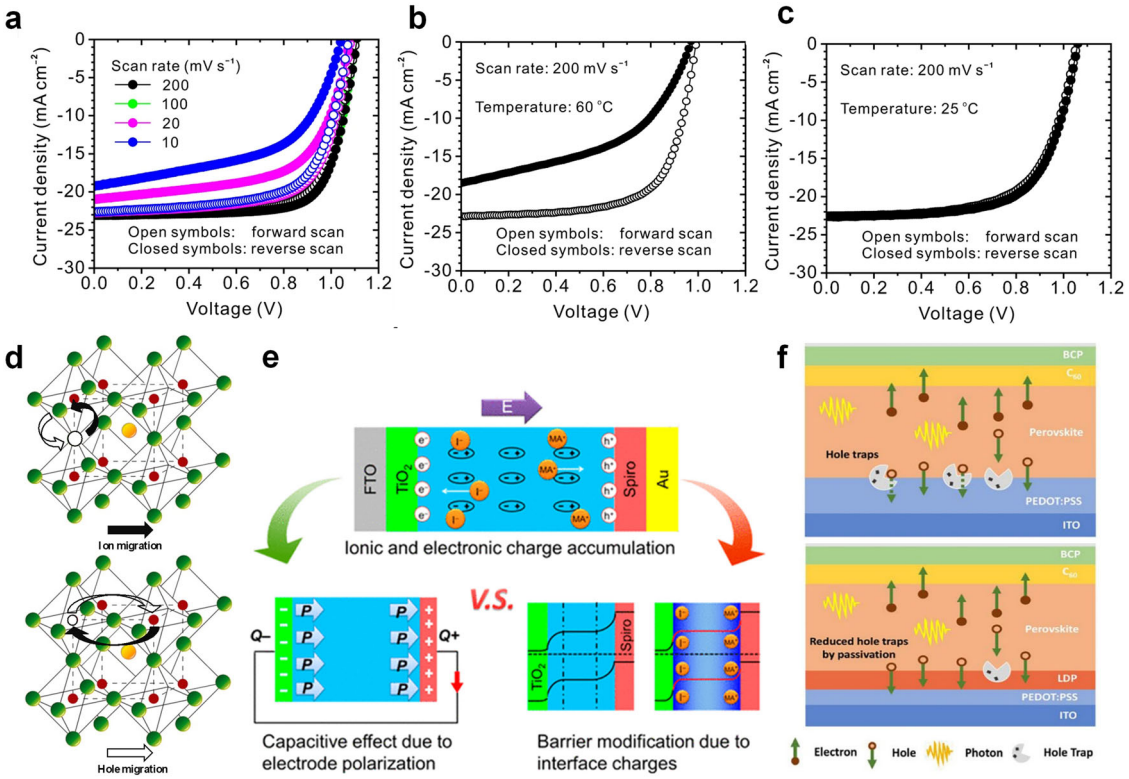

Fig. 7 Influence of the intrinsic factors on the photovoltaic parameters of Sn-HPSCs. a Scan-rate-dependent *J*–*V* curves of PSCs. Effect of temperature on the hysteresis of PSCs at a fast scan rate of 200 mV/s; *J*–*V* curves measured **b** at 60 °C and **c** after cooling to room temperature. Schematic illustrations of **d** ion and hole migration due to iodide vacancies (top) and metal vacancies (bottom) through the perovskite structure, **e** the influence of modifying electrode polarisation on capacitive effect, the impact of contact barrier modification due to ionic interface charges, **f** the surface recombination reduction by passivating the trap states. (Fig. 7 a–c adapted with permission from ref. [109], Copyright 2020 Springer Nature. Fig 7d adapted with permission from ref. [136], Copyright 2015 Royal Society of Chemistry Fig. 7e adapted with permission from ref. [112], Copyright ACS Publications. Figure 7f reproduced with permission from ref. [120], Copyright 2021 MDPI).

Another intrinsic factor for the low efficiency and stability is the electrode polarisation, that is ascribed to the capacitance effect, which depends on the thickness of the layers at the interface. The inefficient extraction of photogenerated carriers causes an accumulation of charges at the perovskite/electrode interface, inducing an electronic dipole polarisation and the subsequent increase in the capacitance[112]. Figure 7d shows the change of electrode polarisation due to the accumulated charges at the interface.

Finally, the trap density at the interface also influences the apparition of the hysteresis (Fig. 7f)[114, 116, 118–120]. Therefore, one strategy is to reduce the non-radiative recombination by lowering the interfacial trap density. Also, lessening the non-steady-state photocurrent by the effect of remanent capacitance current (capacitive effect) and ion migration improves HI in the PSCs. Moreover, engineering to tune the Fermi-level between the CSL and the perovskite materials can enhance the performance of the devices.

Encapsulation

Among the different factors discussed in the previous section, the instability of Sn-HPs caused by oxidative stress is the most challenging issue for commercialising this technology. Proper technological development of encapsulation materials and processes is therefore vital to preserve the stability of Sn-HP. The parameters that define the efficiency of the protective encapsulant are the oxygen transmission rate (OTR) and the water vapour transmission rate (WVTR), which is widely reported and could be taken as a single reference since the two OTR and WVTR values largely correlate.

In the case of rigid devices (prepared on glass or silicon solar cells, for instance), the glass encapsulation employing a properly selected sealant and eventually a desiccator should guarantee an adequate encapsulation. For Pb-HPs, this improves the operational stability of solar cells dramatically[121–123]. Care must be devoted to the sealant's chemical compatibility and mechanical properties; however, we are confident that the main achievement demonstrated with Pb-HPs could be transferred to tin counterparts[124].

The situation is different when considering flexible solar cells[125]. Here, the replacement of lead with less toxic materials is of greater importance, assuming future commercialisation in consumer electronics (e.g., wearable devices). Still, it is not clear which value of OTR should be pursued. In Fig. 8a, we report the target values of OTR and WVTR used for different applications. While plastic foil can quickly meet food packaging, there is a need for ultra-high barriers for air sensitive organic light emitting diodes (OLEDs), that required OTRs and WVTRs below 10^{-6} $cm^3 \cdot m^{-2}$/day and 10^{-6} $g \cdot m^{-2}$/day, respectively[126]. Pb-HPSCs are considered less demanding than OLED in terms of barrier properties. However, this would be hardly true for Sn-HPSCs. Therefore, OLED encapsulation should be the reference technology to look for.

The development of ultra-high barriers taught us that a single layer flexible encapsulant tends to be insufficient. Organic materials have a large permeability intrinsically, while inorganic materials' barrier properties are affected by the presence of pinholes. The best

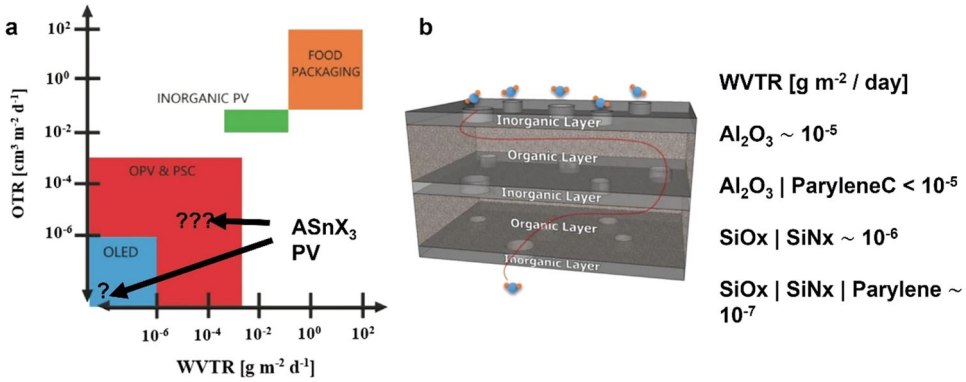

Fig. 8 The OTR and WVTR values required for different applications and the schematic representation of an encapsulating layer. a Oxygen transmission rate and water vapour transmission rate required for different photovoltaic technologies. Food packaging is introduced as a comparison. We note that PSC is considered as lead-based from reference. No estimation is available concerning Sn-HPs PV. **b** The concept of pinhole decoupling is required in ultra-high barriers, where inorganic and organic thin films are sequentially stacked along with the best values taken from ref. [126] (Fig. 8a adapted with permission from ref. [125], Copyright 2021 Wiley. Figure 8b reprinted with permission from ref. [137], Copyright 2018 Springer Nature).

values have been obtained with atomic layer deposition-processed Al_2O_3 with a WVTR approaching 10^{-5} g·m^{-2}/day[127]. Increasing the thickness of a single layer enhances the barrier quality, but only up to a specific value since excessively thick films lose the mechanical properties required for the flexible application. Multi-stacking of thin films is up to date the best option to combine the mechanical properties of organic materials with the barrier properties of inorganic ones. Additionally, the multilayer approach minimises the effect of pinholes in the inorganic layers minimising the probability of finding two of them aligned through two (or more) different layers (Fig. 8b). The best WVTR values reported in the literature fall within 10^{-6}–10^{-7} g·m^{-2}/day, allowing the commercialisation of OLEDs[128, 129]. Still, a dedicated investigation on the suitability for Sn-HP photovoltaics is missing. It would be of great relevance to assess whether further improvements are required or not and what would be the impact on the final levelized cost of energy of the encapsulant. Additionally, we are not aware of investigations concerning the compatibility of Sn-HPs with atomic layer deposition of Al_2O_3 or the chemical vapour deposition of SiO_x, which are mandatory ingredients for the construction of ultra-high barriers, but might induce oxidation on the surface of the Sn-HP.

Outlook

In this review, we have analysed the status of the different strategies followed to improve the performance and stability of Sn-based PSC. One of the most effective strategies has been focused on compositional engineering; the incorporation of inorganic cations or bulky organic cations into Sn-HPs devices have demonstrated a reduction of the formation of volatile products or irreversible disproportion and passivation of the surface defects, respectively, increasing the material stability. Therefore, a deeper understanding of the contribution of organic/inorganic cations in the perovskite composition will contribute to higher PCEs and long-term stability.

In a similar manner, the CSLs also play a crucial role. Most commercial CSLs suffer from having misaligned energy bands with the Sn-HP photoactive material. Recently, the use of self-assembled molecules as hole transport materials has become a hot topic for lead-based perovskite solar cells because it increases the stability and performance of the devices by promoting the formation of uniform films of perovskite and by increasing the hole extraction ability of the CSL[130]. In a similar manner, Song et al. have reported in 2021 the same strategy for Sn-HPSCs, that have attained during 1900 h 80% of the initial PCE without encapsulation[131]. Therefore, the design of novel charge selective molecules with suitable energy alignment specifically for Sn-HPSCs should be considered, minimising their ability to oxidise Sn(II) and the subsequent formation of trap states that lower the Voc. Other sources of trap defects are the interfacial quality of the contact between CSLs and the perovskite photoactive material or the exposure to environmental factors such as humidity, oxygen, temperature, or light. Novel approaches such as solvent engineering, the use of additives, or non-halide reducing agents have improved the performance of Sn-HPSCs, through the control of the crystallisation or the reduction of oxidation reactions in Sn(II). Yang et al have addressed the oriented crystallisation of the Sn-HPs using floating self-assembly molecules that have provided the driving force for an oriented vertical crystallisation of the Sn-HP that has improved the charge extraction[132]. Therefore, research on innovative solvent systems and gaining deeper understanding of the impact of the additives in Sn-HP structures will pave the way for developing new strategies to improve photovoltaic performance.

Finally, we still need to consider the upscaling towards large-area devices and potential high throughput production of devices. Similar to the awareness observed in the fields of Pb-HPSCs or organic photovoltaics, the use of proper encapsulants will be primordial for avoiding the exposure to environmental degradation factors. On the other hand, the development of stable and non-toxic solutions of the reagents will contribute to the deposition of the materials by solution techniques, ideally in air, which will reduce the production costs allowing for coating higher areas of substrates.

Lead-free Sn-HPSCs have shown outstanding and continued progress over Pb-HPSCs since their first reports in 2014. Its lower environmental toxicity and close-to-ideal bandgap values are attracting attention for building efficient, non-toxic stable photovoltaic devices. However, the current situation is that Sn-HPSCs face major stability issues owing to the poor stability of Sn(II) and the unregulated crystallisation rate. These notorious drawbacks still hitch the indisputable potential of tin materials to replace toxic lead. In this review, we have analysed the weaknesses of these devices, which one of the main is Sn(II) oxidation, and how the composition of the perovskite and the device architecture influence the performance of the device. Moreover, we have also described the effect that intrinsic factors, such as ion migration, and the sensitivity of Sn-HP towards environmental conditions have in the PCE and the long-term stability of the devices. Finally, we have exposed the research topics that need to be addressed in order to produce highly stable and efficient Sn-HPSCs.

In conclusion, we believe that the information reported in this review will help to understand the drawbacks that limit efficiency and stability in Sn-HPCs and will contribute towards further development of these devices so they can achieve their full potential to replace lead-based PSCs.

Received: 3 June 2022; Accepted: 12 December 2022;
Published online: 23 December 2022

References

1. NREL. Best Research-Cell Efficiency Chart. https://www.nrel.gov/pv/cell-efficiency.html (2022).
2. Ponti, C. et al. Environmental lead exposure from halide perovskites in solar cells. *Trends Ecol. Evol.* **37**, 281–283 (2022).
3. Li, J. et al. Biological impact of lead from halide perovskites reveals the risk of introducing a safe threshold. *Nat. Commun.* **11**, 1–5 (2020).
4. Filippetti, A. et al. Fundamentals of tin iodide perovskites: a promising route to highly efficient, lead-free solar cells. *J. Mater. Chem. A* **9**, 11812–11826 (2021).
5. Takahashi, Y., Hasegawa, H., Takahashi, Y. & Inabe, T. Hall mobility in tin iodide perovskite CH3NH3SnI 3: Evidence for a doped semiconductor. *J. Solid State Chem.* **205**, 39–43 (2013).
6. Saidaminov, M. I. et al. Conventional solvent oxidizes Sn(II) in perovskite inks. *ACS Energy Lett.* **5**, 1153–1155 (2020).
7. Pascual, J. et al. Origin of Sn(ii) oxidation in tin halide perovskites. *Mater. Adv.* **1**, 1066–1070 (2020).
8. Jiang, X. et al. One-step synthesis of SnI_2·$(DMSO)_x$ adducts for high-performance tin perovskite solar cells. *J. Am. Chem. Soc.* **143**, 10970–10976 (2021).
9. Saliba, M. et al. Cesium-containing triple cation perovskite solar cells: improved stability, reproducibility and high efficiency. *Energy Environ. Sci.* **9**, 1989–1997 (2016).
10. Wang, F. et al. 2D-Quasi-2D-3D hierarchy structure for tin perovskite solar cells with enhanced efficiency and stability. *Joule* **2**, 2732–2743 (2018).
11. Liu, X. et al. Templated growth of FASnI3 crystals for efficient tin perovskite solar cells. *Energy Environ. Sci.* **13**, 2896–2902 (2020).
12. Yu, B. B. et al. Heterogeneous 2D/3D tin-halides perovskite solar cells with certified conversion efficiency breaking 14%. *Adv. Mater.* **33**, 2102055 (2021).
13. Smith, I. C., Hoke, E. T., Solis-Ibarra, D., McGehee, M. D. & Karunadasa, H. I. A layered hybrid perovskite solar-cell absorber with enhanced moisture stability. *Angew. Chem. Int. Ed.* **53**, 11232–11235 (2014).
14. Lanzetta, L. et al. Degradation mechanism of hybrid tin-based perovskite solar cells and the critical role of tin (IV) iodide. *Nat. Commun.* https://doi.org/10.1038/s41467-021-22864-z (2021).
15. Juarez-Perez, E. J., Hawash, Z., Raga, S. R., Ono, L. K. & Qi, Y. Thermal degradation of CH3NH3PbI3 perovskite into NH3 and CH3I gases observed by coupled thermogravimetry–mass spectrometry analysis. *Energy Environ. Sci.* **9**, 3406–3410 (2016).
16. Cao, J. & Yan, F. Recent progress in tin-based perovskite solar cells. *Energy Environ. Sci.* **14**, 1286–1325 (2021).
17. Shi, T. et al. Effects of organic cations on the defect physics of tin halide perovskites. *J. Mater. Chem. A* **5**, 15124–15129 (2017).
18. Berhe, T. A. et al. Organometal halide perovskite solar cells: degradation and stability. *Energy Environ. Sci.* **9**, 323–356 (2016).
19. Akbulatov, A. F. et al. Comparative intrinsic thermal and photochemical stability of Sn(II) complex halides as next-generation materials for lead-free perovskite solar cells. *J. Phys. Chem. C* **123**, 26862–26869 (2019).
20. Akbulatov, A. F. et al. Probing the intrinsic thermal and photochemical stability of hybrid and inorganic lead halide perovskites. *J. Phys. Chem. Lett.* **8**, 1211–1218 (2017).
21. Dalpian, G. M. et al. Changes in charge density vs changes in formal oxidation states: the case of Sn halide perovskites and their ordered vacancy analogues. *Phys. Rev. Mater.* **1**, 1–10 (2017).
22. El-Mellouhi, F. et al. Hydrogen bonding and stability of hybrid organic-inorganic perovskites. *ChemSusChem* **9**, 2648–2655 (2016).
23. Zhao, Z. et al. Mixed-organic-cation tin iodide for lead-free perovskite solar cells with an efficiency of 8.12%. *Adv. Sci.* **4**, 1700204 (2017).
24. Tsai, C. M. et al. Control of crystal structures and optical properties with hybrid formamidinium and 2-hydroxyethylammonium cations for mesoscopic carbon-electrode tin-based perovskite solar cells. *ACS Energy Lett.* **3**, 2077–2085 (2018).
25. Wang, F. et al. Organic cation-dependent degradation mechanism of organotin halide perovskites. *Adv. Funct. Mater.* **26**, 3417–3423 (2016).
26. Jokar, E. et al. Slow surface passivation and crystal relaxation with additives to improve device performance and durability for tin-based perovskite solar cells. *Energy Environ. Sci.* **11**, 2353–2362 (2018).
27. Diau, E. W. G., Jokar, E. & Rameez, M. Strategies to improve performance and stability for tin-based perovskite solar cells. *ACS Energy Lett.* **4**, 1930–1937 (2019).
28. Jokar, E., Chien, C. H., Tsai, C. M., Fathi, A. & Diau, E. W. G. Robust tin-based perovskite solar cells with hybrid organic cations to attain efficiency approaching 10%. *Adv. Mater.* **31**, 1–7 (2019).
29. Jokar, E. et al. Mixing of azetidinium in formamidinium tin triiodide perovskite solar cells for enhanced photovoltaic performance and high stability in air. *ChemSusChem* **14**, 4415–4421 (2021).
30. Saliba, M. et al. Cesium-containing triple cation perovskite solar cells: improved stability, reproducibility and high efficiency. *Energy Environ. Sci.* **9**, 1989–1997 (2016).
31. Liu, X. et al. Improved efficiency and stability of Pb–Sn binary perovskite solar cells by Cs substitution. *J. Mater. Chem. A* **4**, 17939–17945 (2016).
32. Liu, X. et al. Efficient and stable tin perovskite solar cells enabled by amorphous-polycrystalline structure. *Nat. Commun.* **11**, 1–7 (2020).
33. Wu, T. et al. Lead-free tin perovskite solar cells. *Joule* **5**, 863–886 (2021).
34. Wang, J. et al. Controlling the crystallization kinetics of lead-free tin halide perovskites for high performance green photovoltaics. *Adv. Energy Mater.* **11**, 1–18 (2021).
35. Tsai, H. et al. High-efficiency two-dimensional Ruddlesden–Popper perovskite solar cells. *Nature* **536**, 312–316 (2016).
36. Liao, Y. et al. Highly oriented low-dimensional tin halide perovskites with enhanced stability and photovoltaic performance. *J. Am. Chem. Soc.* **139**, 6693–6699 (2017).
37. Zhu, P., Chen, C., Gu, S., Lin, R. & Zhu, J. CsSnI3 solar cells via an evaporation-assisted solution method. *Sol. RRL* **2**, 1700224 (2018).
38. Qiu, J. et al. 2D intermediate suppression for efficient Ruddlesden-Popper (RP) phase lead-free perovskite solar cells. *ACS Energy Lett.* **4**, 1513–1520 (2019).
39. Li, H. et al. Low-dimensional inorganic tin perovskite solar cells prepared by templated growth. *Angew. Chem. - Int. Ed.* **60**, 16330–16336 (2021).
40. Nishimura, K. et al. Lead-free tin-halide perovskite solar cells with 13% efficiency. *Nano Energy* **74**, 104858 (2020).
41. Wang, C. et al. Illumination durability and high-efficiency Sn-based perovskite solar cell under coordinated control of phenylhydrazine and halogen ions. *Matter* **4**, 709–721 (2021).
42. Jokar, E. et al. Enhanced performance and stability of 3D/2D tin perovskite solar cells fabricated with a sequential solution deposition. *ACS Energy Lett.* **6**, 485–492 (2021).
43. Liao, M. et al. Efficient and stable FASnI3 perovskite solar cells with effective interface modulation by low-dimensional perovskite layer. *ChemSusChem* **12**, 5007–5014 (2019).
44. Choi, W. G., Park, C. G., Kim, Y. & Moon, T. Sn perovskite solar cells via 2D/3D bilayer formation through a sequential vapor process. *ACS Energy Lett.* **5**, 3461–3467 (2020).
45. Chen, B. et al. Reducing the interfacial voltage loss in tin halides perovskite solar cells. *Chem. Eng. J.* **445**, 136769 (2022).
46. Jokar, E. et al. Slow passivation and inverted hysteresis for hybrid tin perovskite solar cells attaining 13.5% via sequential deposition. *J. Phys. Chem. Lett.* **12**, 10106–10111 (2021).
47. Pitaro, M., Tekelenburg, E. K., Shao, S. & Loi, M. A. Tin halide perovskites: from fundamental properties to solar cells. *Adv. Mater.* **34**, 2105844 (2021)
48. Li, M. et al. Advances in Tin(II)-based perovskite solar cells: from material physics to device performance. *Small Struct.* **3**, 2100102 (2022).
49. Koh, T. M. et al. Formamidinium tin-based perovskite with low Eg for photovoltaic applications. *J. Mater. Chem. A* **3**, 14996–15000 (2015).
50. Jiang, X. et al. Ultra-high open-circuit voltage of tin perovskite solar cells via an electron transporting layer design. *Nat. Commun.* **11**, 1–7 (2020).
51. Wang, N. et al. Heterojunction-depleted lead-free perovskite solar cells with coarse-grained B-γ-CsSnI3 thin films. *Adv. Energy Mater.* **6**, 1601130 (2016).
52. Aldamasy, M. et al. Challenges in tin perovskite solar cells. *Phys. Chem. Chem. Phys.* **23**, 23413–23427 (2021).
53. Tao, S. et al. Absolute energy level positions in tin- and lead-based halide perovskites. *Nat. Commun.* **10**, 1–10 (2019).
54. Noel, N. K. et al. Lead-free organic-inorganic tin halide perovskites for photovoltaic applications. *Energy Environ. Sci.* **7**, 3061–3068 (2014).
55. Hao, F., Stoumpos, C. C., Cao, D. H., Chang, R. P. H. & Kanatzidis, M. G. Lead-free solid-state organic-inorganic halide perovskite solar cells. *Nat. Photonics* **8**, 489–494 (2014).
56. Hao, F., Stoumpos, C. C., Chang, R. P. H. & Kanatzidis, M. G. Anomalous band gap behavior in mixed Sn and Pb perovskites enables broadening of absorption spectrum in solar cells. *J. Am. Chem. Soc.* **136**, 8094–8099 (2014).

57. Lee, S. J. et al. Reducing carrier density in formamidinium tin perovskites and its beneficial effects on stability and efficiency of perovskite solar cells. *ACS Energy Lett.* **3**, 46–53 (2018).
58. Duong, T. et al. Efficient and stable wide bandgap perovskite solar cells through surface passivation with long alkyl chain organic cations. *J. Mater. Chem. A* **9**, 18454–18465 (2021).
59. Mahmoudi, T. et al. Suppression of Sn2+/Sn4+ oxidation in tin-based perovskite solar cells with graphene-tin quantum dots composites in active layer. *Nano Energy* **90**, 106495 (2021).
60. Hu, M. et al. Regulating the surface passivation and residual strain in pure tin perovskite films. *ACS Energy Lett.* **6**, 3555–3562 (2021).
61. Zhang, X. et al. The voltage loss in tin halide perovskite solar cells: origins and perspectives. *Adv. Funct. Mater.* **2108832**, 1–17 (2021).
62. Tang, H., Shang, Y., Zhou, W., Peng, Z. & Ning, Z. Energy level tuning of PEDOT:PSS for high performance tin-lead mixed perovskite solar cells. *Sol. RRL* **3**, 1800256 (2019).
63. Yang, W.-F. et al. Nicotinamide-modified PEDOT:PSS for high performance indoor and outdoor tin perovskite photovoltaics. *Sol. RRL* **5**, 2100713 (2021).
64. Liu, X., Wang, Y., Xie, F., Yang, X. & Han, L. Improving the performance of inverted formamidinium tin iodide perovskite solar cells by reducing the energy-level mismatch. *ACS Energy Lett* **3**, 1116–1121 (2018).
65. Ran, C. et al. Bilateral interface engineering toward efficient 2D–3D bulk heterojunction tin halide lead-free perovskite solar cells. *ACS Energy Lett* **3**, 713–721 (2018).
66. Shih, C.-C. & Wu, C.-G. Synergistic engineering of the conductivity and surface properties of PEDOT:PSS-Based HTLs for inverted tin perovskite solar cells to achieve efficiency over 10%. *ACS Appl. Mater. Interfaces* **14**, 16125–16135 (2022).
67. Roose, B., Wang, Q. & Abate, A. The role of charge selective contacts in perovskite solar cell stability. *Adv. Energy Mater.* **9**, 1803140 (2018)
68. Miyamoto, Y. et al. High current density Sn-based perovskite solar cells via enhanced electron extraction in nanoporous electron transport layers. *ACS Appl. Nano Mater* **3**, 11650–11657 (2020).
69. Li, M. et al. Tin halide perovskite films made of highly oriented 2D crystals enable more efficient and stable lead-free perovskite solar cells. *ACS Energy Lett.* **5**, 1923–1929 (2020).
70. Chen, M. et al. High-performance lead-free solar cells based on tin-halide perovskite thin films functionalized by a divalent organic cation. *ACS Energy Lett.* **5**, 2223–2230 (2020).
71. Cao, J. et al. Enhanced performance of tin-based perovskite solar cells induced by an ammonium hypophosphite additive. *J. Mater. Chem. A* **7**, 26580–26585 (2019).
72. Wang, T. et al. Highly air-stable tin-based perovskite solar cells through grain-surface protection by gallic acid. *ACS Energy Lett.* **5**, 1741–1749 (2020).
73. Wijesekara, A. et al. Enhanced stability of tin halide perovskite photovoltaics using a Bathocuproine—copper top electrode. *Adv. Energy Mater.* **11**, 2102766 (2021).
74. Li, B. et al. Tin-based defects and passivation strategies in tin-related perovskite solar cells. *ACS Energy Lett.* **5**, 3752–3772 (2020).
75. Pascual, J. et al. Lights and shadows of DMSO as solvent for tin halide perovskites. *Chem. – A Eur. J.* **28**, e202103919 (2022).
76. Hao, F. et al. Solvent-mediated crystallization of CH3NH3SnI3 films for heterojunction depleted perovskite solar cells. *J. Am. Chem. Soc.* **137**, 11445–11452 (2015).
77. Di Girolamo, D. et al. Solvents for processing stable tin halide perovskites. *ACS Energy Lett.* **6**, 959–968 (2021).
78. Kumar, M. H. et al. Lead-free halide perovskite solar cells with high photocurrents realized through vacancy modulation. *Adv. Mater.* **26**, 7122–7127 (2014).
79. Konstantakou, M. & Stergiopoulos, T. A critical review on tin halide perovskite solar cells. *J. Mater. Chem. A* **5**, 11518–11549 (2017).
80. Gupta, S., Bendikov, T., Hodes, G. & Cahen, D. CsSnBr3, a lead-free halide perovskite for long-term solar cell application: insights on SnF2 addition. *ACS Energy Lett* **1**, 1028–1033 (2016).
81. Kontos, A. G. et al. Structural stability, vibrational properties, and photoluminescence in CsSnI3 perovskite upon the addition of SnF2. *Inorg. Chem.* **56**, 84–91 (2017).
82. Milot, R. L. et al. The effects of doping density and temperature on the optoelectronic properties of formamidinium tin triiodide thin films. *Adv. Mater.* **30**, 1804506 (2018).
83. Pascual, J. et al. Fluoride chemistry in tin halide perovskites. *Angew. Chem. Int. Ed.* **60**, 21583–21591 (2021).
84. Ricciarelli, D., Meggiolaro, D., Ambrosio, F., & De Angelis, F. Instability of tin iodide perovskites: bulk p-doping versus surface tin oxidation. *ACS Energy Lett.* **5**, 2787–2795 (2020).
85. Marshall, K. P., Walker, M., Walton, R. I. & Hatton, R. A. Enhanced stability and efficiency in hole-transport-layer-free CsSnI3 perovskite photovoltaics. *Nat. Energy* **1**, 16178 (2016).
86. Tai, Q. et al. Antioxidant grain passivation for air-stable tin-based perovskite solar cells. *Angew. Chem. - Int. Ed.* **58**, 806–810 (2019).
87. Dai, Z. et al. Stable tin perovskite solar cells developed via additive engineering. *Sci. China Mater.* **64**, 2645–2654 (2021).
88. Gu, F. et al. Tin(II) acetylacetonate as a new type of tin compensator additive for tin-based perovskite solar cells. *ACS Appl. Mater. Interfaces* **13**, 44157–44164 (2021).
89. Rameez, M. et al. Development of hybrid pseudohalide tin perovskites for highly stable carbon-electrode solar cells. *ACS Appl. Mater. Interfaces* **12**, 21739–21747 (2020).
90. Tang, G. et al. Synergistic effects of the zinc acetate additive on the performance enhancement of Sn-based perovskite solar cells. *Mater. Chem. Front.* **5**, 1995–2000 (2021).
91. Wang, C. et al. Illumination durability and high-efficiency Sn-based perovskite solar cell under coordinated control of phenylhydrazine and halogen ions. *Matter* **4**, 709–721 (2021).
92. Kayesh, M. E. et al. Enhanced photovoltaic performance of FASnI3-based perovskite solar cells with hydrazinium chloride coadditive. *ACS Energy Lett.* **3**, 1584–1589 (2018).
93. Wang, C. et al. Self-repairing tin-based perovskite solar cells with a breakthrough efficiency over 11%. *Adv. Mater.* **32**, 1–9 (2020).
94. Li, W. et al. Addictive-assisted construction of all-inorganic CsSnIBr2 mesoscopic perovskite solar cells with superior thermal stability up to 473 K. *J. Mater. Chem. A* **4**, 17104–17110 (2016).
95. Meng, X. et al. Highly reproducible and efficient FASnI3 perovskite solar cells fabricated with volatilizable reducing solvent. *J. Phys. Chem. Lett.* **11**, 2965–2971 (2020).
96. Sanchez-Diaz, J. et al. Tin perovskite solar cells with >1300 h of operational stability in N2 through a synergistic chemical engineering approach. *Joule* **6**, 1–23 (2022).
97. Gu, F. et al. Improving performance of lead-free formamidinium tin triiodide perovskite solar cells by tin source purification. *Sol. RRL* **2**, 1800136 (2018).
98. Nakamura, T. et al. Sn(IV)-free tin perovskite films realized by in situ Sn(0) nanoparticle treatment of the precursor solution. *Nat. Commun.* **11**, 1–8 (2020).
99. Aftab, A. & Ahmad, M. I. A review of stability and progress in tin halide perovskite solar cell. *Sol. Energy* **216**, 26–47 (2021).
100. Xie, G. et al. Insight into the reaction mechanism of water, oxygen, and nitrogen molecules on a tin iodine perovskite surface. *J. Mater. Chem. A* **7**, 5779–5793 (2019).
101. Li, W. et al. Phase stability and impact of water on CsSnI3 perovskite. *Appl. Phys. Express* **13**, 071003 (2020).
102. Li, Z., Ji, J., Zhang, C., Hou, Q. & Jin, P. First-principles study on the oxygen–light-induced iodide vacancy formation in FASnI3 perovskite. *J. Phys. Chem. C* **124**, 14147–14157 (2020).
103. Gao, W. et al. Robust stability of efficient lead-free formamidinium tin iodide perovskite solar cells realized by structural regulation. *J. Phys. Chem. Lett.* **9**, 6999–7006 (2018).
104. Zhang, M. et al. Recent progress in inorganic tin perovskite solar cells. *Mater Today Energy* **23**, 100891 (2022).
105. Leijtens, T. et al. Overcoming ultraviolet light instability of sensitized TiO2 with meso-superstructured organometal tri-halide perovskite solar cells. *Nat. Commun.* **4**, 2885 (2013).
106. Dixit, H. et al. Assessment of lead-free tin halide perovskite solar cells using *J–V* hysteresis. *Phys. Status Solidi* **219**, 2100823 (2022)
107. Li, J. et al. Pinning bromide ion with ionic liquid in lead-free Cs2AgBiBr6 double perovskite solar cells. *Adv. Funct. Mater.* **32**, 2112991 (2022)
108. Shao, S. et al. Highly reproducible Sn-based hybrid perovskite solar cells with 9% efficiency. *Adv. Energy Mater.* **8**, 1702019 (2018).
109. Tumen-Ulzii, G. et al. Hysteresis-less and stable perovskite solar cells with a self-assembled monolayer. *Commun. Mater.* **1**, 1–7 (2020).
110. Rong, Y. et al. Tunable hysteresis effect for perovskite solar cells. *Energy Environ. Sci.* **10**, 2383–2391 (2017).
111. Yu, Y. et al. Thermally evaporated methylammonium tin triiodide thin films for lead-free perovskite solar cell fabrication. *RSC Adv.* **6**, 90248–90254 (2016).
112. Chen, B. et al. Impact of capacitive effect and ion migration on the hysteretic behavior of perovskite solar cells. *J. Phys. Chem. Lett.* **6**, 4693–4700 (2015).
113. Dunbar, R. B. et al. How reliable are efficiency measurements of perovskite solar cells? The first inter-comparison, between two accredited and eight non-accredited laboratories. *J. Mater. Chem. A* **5**, 22542–22558 (2017).
114. Aygüler, M. F. et al. Influence of Fermi level alignment with tin oxide on the hysteresis of perovskite solar cells. *ACS Appl. Mater. Interfaces* **10**, 11414–11419 (2018).
115. Ansari, M. I. H., Qurashi, A. & Nazeeruddin, M. K. Frontiers, opportunities, and challenges in perovskite solar cells: a critical review. *J. Photochem. Photobiol. C Photochem. Rev.* **35**, 1–24 (2018).
116. Calado, P. et al. Evidence for ion migration in hybrid perovskite solar cells with minimal hysteresis. *Nat. Commun.* **7**, 13831 (2016).

117. Rajagopal, A., Yao, K. & Jen, A. K. -Y. Toward perovskite solar cell commercialization: a perspective and research roadmap based on interfacial engineering. *Adv. Mater.* **30**, 1800455 (2018).
118. Shao, Y., Xiao, Z., Bi, C., Yuan, Y. & Huang, J. Origin and elimination of photocurrent hysteresis by fullerene passivation in CH3NH3PbI3 planar heterojunction solar cells. *Nat. Commun.* **5**, 1–7 (2014).
119. Liu, H. et al. Dopants for enhanced performance of tin-based perovskite solar cells—a short review. *Coatings* **11**, 1–14 (2021).
120. Chen, K. et al. Low-dimensional perovskite interlayer for highly efficient lead-free formamidinium tin iodide perovskite solar cells. *Nano Energy* **49**, 411–418 (2018).
121. Cheacharoen, R. et al. Design and understanding of encapsulated perovskite solar cells to withstand temperature cycling. *Energy Environ. Sci.* **11**, 144–150 (2018).
122. Cheacharoen, R. et al. Encapsulating perovskite solar cells to withstand damp heat and thermal cycling. *Sustain. Energy Fuels* **2**, 2398–2406 (2018).
123. Matteocci, F. et al. Encapsulation for long-term stability enhancement of perovskite solar cells. *Nano Energy* **30**, 162–172 (2016).
124. Wang, Y. et al. Encapsulation and stability testing of perovskite solar cells for real life applications. *ACS Mater. Au* **2**, 215–236 (2022).
125. Sutherland, L. J., Weerasinghe, H. C. & Simon, G. P. A review on emerging barrier materials and encapsulation strategies for flexible perovskite and organic photovoltaics. *Adv. Energy Mater.* **11**, 2101383 (2021).
126. Lu, Q. et al. A review on encapsulation technology from organic light emitting diodes to organic and perovskite solar cells. *Adv. Funct. Mater.* **31**, 2100151 (2021).
127. Carcia, P. F., McLean, R. S., Reilly, M. H., Groner, M. D. & George, S. M. Ca test of Al2O3 gas diffusion barriers grown by atomic layer deposition on polymers. *Appl. Phys. Lett.* **89**, 031915 (2006).
128. Wu, J. et al. Efficient multi-barrier thin film encapsulation of OLED using alternating Al2O3 and polymer layers. *RSC Adv.* **8**, 5721–5727 (2018).
129. Chen, T.-N. et al. Improvements of permeation barrier coatings using encapsulated parylene interlayers for flexible electronic applications. *Plasma Process. Polym.* **4**, 180–185 (2007).
130. Aktas, E. et al. Understanding the perovskite/self-assembled selective contact interface for ultra-stable and highly efficient p–i–n perovskite solar cells. *Energy Environ. Sci.* **14**, 3976–3985 (2021).
131. Song, D., Narra, S., Li, M. Y., Lin, J. S. & Diau, E. W. G. Interfacial engineering with a hole-selective self-assembled monolayer for tin perovskite solar cells via a two-step fabrication. *ACS Energy Lett.* **6**, 4179–4186 (2021).
132. Yang, J. et al. Directional crystallization by floating self-assembly for efficient and stable tin-based perovskite solar cells. *Chem. Mater.* **33**, 4362–4372 (2021).
133. Kayesh, M. E. et al. Coadditive engineering with 5-ammonium valeric acid iodide for efficient and stable Sn perovskite solar cells. *ACS Energy Lett.* **4**, 278–284 (2019).
134. He, X. et al. Highly efficient tin perovskite solar cells achieved in a wide oxygen concentration range. *J. Mater. Chem. A* **8**, 2760–2768 (2020).
135. Aktas, E. Low-molecular weight molecules as selective contacts for perovskite solar cells. http://hdl.handle.net/10803/672777 (2021).
136. Azpiroz, J. M., Mosconi, E., Bisquert, J. & De Angelis, F. Defect migration in methylammonium lead iodide and its role in perovskite solar cell operation. *Energy Environ. Sci.* **8**, 2118–2127 (2015).
137. Lee, S., Han, J.-H., Lee, S.-H., Baek, G.-H. & Park, J.-S. Review of organic/inorganic thin film encapsulation by atomic layer deposition for a flexible OLED display. *JOM* **71**, 197–211 (2019).

Acknowledgements

This work has received funding from the European Research Council (ERC) under the European Union's Horizon 2020 research and innovation programme (Grant agreement No. 804519). E.A. is supported by the project that has received funding from the European Union's Horizon 2020 research and innovation programme under the Marie Skłodowska-Curie grant agreement No 956270. A.W. thanks the financial support from JST–ALCA (JPMJAL1603). E.M.F. and E.P. thank MINECO (project PID2019-109389RB-I00) and MCIN/AEI for funding through the project SOL FUTURE (PLEC2021-007906) with the help of NextGenerationEU/ PRTR. W.L. and E.P. are also thankful to ICIQ, CERCA, and ICREA for financial support. N.R. acknowledges the Marie Skłodowska-Curie European Postdoctoral Fellowships programme (Grant 101028693, SpinPVK).

Author contributions

E.A. and N.R. initiated and wrote this manuscript with contributions from J.P., S.H., M.H.A., D.D.G., W.L., G.N., and E.M.F., supported by A.W., E.P., and A.A. All authors discussed and revised the manuscript and have given approval to its final version.

Competing interests

The authors declare no competing interests.

Additional information

Supplementary information The online version contains supplementary material available at https://doi.org/10.1038/s43246-022-00327-2.

Correspondence and requests for materials should be addressed to Atsushi Wakamiya, Emilio Palomares or Antonio Abate.

Peer review information *Communications Materials* thanks Yanbo Wang, Eric Wei-Guang Diau and the other, anonymous, reviewer for their contribution to the peer review of this work. Primary Handling Editors: Hairen Tan & John Plummer. Peer reviewer reports are available.

Reprints and permission information is available at http://www.nature.com/reprints

Publisher's note Springer Nature remains neutral with regard to jurisdictional claims in published maps and institutional affiliations.